CrossMark

An Isolated Microlens Observed from *K2*, *Spitzer*, and Earth

Wei Zhu (祝伟)[1,2] , A. Udalski[3], C. X. Huang[4] , S. Calchi Novati[5,6], T. Sumi[7], R. Poleski[1,3], J. Skowron[3], P. Mróz[3],
M. K. Szymański[3], I. Soszyński[3], P. Pietrukowicz[3], S. Kozłowski[3], K. Ulaczyk[3,8], M. Pawlak[3]

(OGLE Collaboration),

C. Beichman[9], G. Bryden[10], S. Carey[11], B. S. Gaudi[1], A. Gould[1,12,13], C. B. Henderson[10], Y. Shvartzvald[10,27], J. C. Yee[14]

(Spitzer Team),

and

I. A. Bond[15], D. P. Bennett[16], D. Suzuki[17], N. J. Rattenbury[18], N. Koshimoto[7], F. Abe[19], Y. Asakura[19], R. K. Barry[16],
A. Bhattacharya[16,20], M. Donachie[18], P. Evans[18], A. Fukui[21], Y. Hirao[7], Y. Itow[19], K. Kawasaki[7], M. C. A. Li[18], C. H. Ling[15],
K. Masuda[19], Y. Matsubara[19], S. Miyazaki[7], H. Munakata[19], Y. Muraki[19], M. Nagakane[7], K. Ohnishi[22], C. Ranc[16], To. Saito[23],
A. Sharan[18], D. J. Sullivan[24], P. J. Tristram[25], T. Yamada[26], and A. Yonehara[26]

(MOA Collaboration)

[1] Department of Astronomy, Ohio State University, 140 W. 18th Avenue, Columbus, OH 43210, USA; zhu.908@osu.edu
[2] Canadian Institute for Theoretical Astrophysics, 60 St. George Street, University of Toronto, Toronto, ON M5S 3H8, Canada
[3] Warsaw University Observatory, Al. Ujazdowskie 4, 00-478 Warszawa, Poland
[4] Department of Physics and Kavli Institute for Astrophysics and Space Research, Massachusetts Institute of Technology, Cambridge, MA 02139, USA
[5] IPAC, California Institute of Technology, Mail Code 100-22, 1200 E. California Boulevard, Pasadena, CA 91125, USA
[6] Dipartimento di Fisica "E. R. Caianiello," Università di Salerno, Via Giovanni Paolo II, I-84084 Fisciano (SA), Italy
[7] Department of Earth and Space Science, Graduate School of Science, Osaka University, 1-1 Machikaneyama, Toyonake, Osaka 560-0043, Japan
[8] Department of Physics, University of Warwick, Gibbert Hill Road, Coventry CV4 7AL, UK
[9] NASA Exoplanet Science Institute, California Institute of Technology, MS 100-22, Pasadena, CA 91125, USA
[10] Jet Propulsion Laboratory, California Institute of Technology, 4800 Oak Grove Drive, Pasadena, CA 91109, USA
[11] Spitzer Science Center, California Institute of Technology, MS 220-6, Pasadena, CA, USA
[12] Korea Astronomy and Space Science Institute, 776 Daedeokdae-ro, Yuseong-Gu, Daejeon 34055, Korea
[13] Max-Planck-Institute for Astronomy, Königstuhl 17, D-69117 Heidelberg, Germany
[14] Smithsonian Astrophysical Observatory, 60 Garden Street, Cambridge, MA 02138, USA
[15] Institute for Natural and Mathematical Sciences, Massey University, Private Bag 102904, North Shore Mail Centre, Auckland 0745, New Zealand
[16] Laboratory for Exoplanets and Stellar Astrophysics, NASA Goddard Space Flight Center, Greenbelt, MD 20771, USA
[17] Institute of Space and Astronautical Science, Japan Aerospace Exploration Agency, 3-1-1 Yoshinodai, Chuo, Sagamihara, Kanagawa 252-5210, Japan
[18] Department of Physics, University of Auckland, Private Bag 92019, Auckland, New Zealand
[19] Institute of Space-Earth Environmental Research, Nagoya University, Furo-cho, Chikusa, Nagoya, Aichi 464-8601, Japan
[20] Department of Physics, University of Notre Dame, Notre Dame, IN 46556, USA
[21] Okayama Astrophysical National Astronomical Observatory, 3037-5 Honjo, Kamogata, Asakuchi, Okayama 719-0232, Japan
[22] Nagano National College of Technology, Nagano 381-8550, Japan
[23] Tokyo Metropolitan College of Industrial Technology, Tokyo 116-8523, Japan
[24] School of Chemical and Physical Sciences, Victoria University, Wellington, New Zealand
[25] University of Canterbury Mt John Observatory, P.O. Box 56, Lake Tekapo 7945, New Zealand
[26] Department of Physics, Faculty of Science, Kyoto Sangyo University, Kyoto 603-8555, Japan

Abstract

We present the result of microlensing event MOA-2016-BLG-290, which received observations from the two-wheel *Kepler* (*K2*), *Spitzer*, as well as ground-based observatories. A joint analysis of data from *K2* and the ground leads to two degenerate solutions of the lens mass and distance. This degeneracy is effectively broken once the (partial) *Spitzer* light curve is included. Altogether, the lens is found to be an extremely low-mass star or brown dwarf ($77^{+34}_{-23}\,M_J$) located in the Galactic bulge (6.8 ± 0.4 kpc). MOA-2016-BLG-290 is the first microlensing event for which we have signals from three well-separated ($\sim$1 au) locations. It demonstrates the power of two-satellite microlensing experiment in reducing the ambiguity of lens properties, as pointed out independently by S. Refsdal and A. Gould several decades ago.

Key words: gravitational lensing: micro – methods: data analysis – parallaxes – stars: fundamental parameters – techniques: photometric

1. Introduction

The implementation of the space-based microlensing parallax has revolutionized the field of Galactic microlensing (e.g., Dong et al. 2007; Udalski et al. 2015). The same microlensing event is seen to evolve differently in views of ground-based telescopes and a space-based telescope such as *Spitzer* or *Kepler* because of the large separation ($\sim$1 au; Refsdal 1966; Gould 1994; Gould & Horne 2013). This effect yields the microlensing parallax vector π_E, which conveys crucial information on the lens mass and distance.

Although the *Spitzer* microlensing program has been successful in terms of measuring masses of individual planetary systems (Udalski et al. 2015; Street et al. 2016; Ryu et al. 2017;

---

[27] NASA Postdoctoral Program Fellow.

Shvartzvald et al. 2017) and constraining the Galactic distribution of planets (Calchi Novati et al. 2015a; Yee et al. 2015a; Zhu et al. 2017b), there is a generic uncertainty in measuring π_E with a single satellite, especially in cases of single-lens events. The microlensing parallax vector $\boldsymbol{\pi}_E$ is directly related to the displacement between the two lens-source relative trajectories

$$\boldsymbol{\pi}_E \approx \frac{\mathrm{au}}{D_\perp}\left(\frac{t_{0,\mathrm{sat}} - t_{0,\oplus}}{t_E}, \ u_{0,\mathrm{sat}} - u_{0,\oplus}\right), \tag{1}$$

where $D_\perp$ is the separation between the satellite and Earth perpendicular to the line of sight, t_0 is the time of maximum magnification, u_0 is the impact parameter, and subscripts "sat" and "$\oplus$" denote those seen by the satellite and Earth, respectively. Ambiguities arise because in the majority of cases, only $|u_0|$ (rather than u_0) can be constrained by the light curve, thus leading to a fourfold degeneracy in vector $\boldsymbol{\pi}_E$ and a twofold degeneracy in its amplitude π_E. Several studies have proposed ways to break these degeneracies, and others pointed out special situations in which such degeneracies do not matter (see Yee et al. 2015b and references therein).

Along with proposing the idea of a space-based microlensing parallax, Refsdal (1966) and Gould (1994) also pointed out that the most efficient way to break such parallax degeneracies should be to observe the same microlensing event simultaneously from another well-separated and misaligned location (satellite). The addition of a second satellite can effectively break the parallax degeneracies, especially the amplitude degeneracy.

Several decades after this idea was proposed, we finally have the chance to test it. In 2016, the two-wheel *Kepler* mission (*K2*; Howell et al. 2014) conducted a microlensing campaign toward the Galactic bulge from April 22 to July 2, which overlapped with the *Spitzer* microlensing campaign (June 18 to July 26) for nearly two weeks. With this unique opportunity, a specific program (Gould et al. 2015) was developed in order to demonstrate the idea of Refsdal (1966) and Gould (1994). In total, about 30 microlensing events received observations from both satellites in addition to the dense coverage by ground-based telescopes.[28] This work presents the first analysis of this sample, specifically the bright single-lens event MOA-2016-BLG-290 for which the microlensing signal is detected from all three locations.[29]

2. Observations and Data Reductions

Microlensing event MOA-2016-BLG-290 was first identified by the Microlensing Observations in Astrophysics (MOA; Bond et al. 2001) collaboration at 20:26 UT on 2016 June 1 (HJD$'$ = HJD–2450000 = 7541.35), based on observations from its 1.8 m telescope with a 2.2 deg^2 field at Mt. John, New Zealand. About five days later, this event was also alerted as OGLE-2016-BLG-0975 by the Optical Gravitational

Lensing Experiment (OGLE; Udalski et al. 2015) Collaboration through the Early Warning System (Udalski et al. 1994; Udalski 2003), based on data taken by the 1.3 m Warsaw Telescope at the Las Campanas Observatory in Chile.

With equatorial coordinates (R.A., decl.)$_{2000}$ = (18^{h}04^{m}57^{s}01, $-28°37'40''1$) and Galactic coordinates $(l, b)_{2000}$ = (2°40, $-3°50$), this event lies inside the microlensing super stamp of the *K2* Campaign 9 (Gould & Horne 2013; Henderson et al. 2016). It was therefore monitored at 30 minute cadence by *K2* from 2016 April 22 to May 18 (C9a, HJD$'$=7501–7527) and from May 22 to July 2 (C9b, HJD$'$ = 7531–7572).

Events such as MOA-2016-BLG-290 that were observed by *K2* were preferentially selected during the 2016 *Spitzer* microlensing campaign, for the purpose of demonstrating the two-satellite microlensing parallax concept (Gould et al. 2015). In the current case, the *Spitzer* team selected it as a *Spitzer* target subjectively at UT 15:03 on 2016 June 9 (HJD$'$ = 7549.13), following a revised protocol of Yee et al. (2015a). This selection turned into objective on June 12, meaning that this event met our objective selection criteria. Because of the Sun-angle limit, the *Spitzer* observations were taken between HJD$'$ = 7559.6 and 7571.2 at a quasi-daily cadence. All *Spitzer* observations were taken in the 3.6 μm channel.

The ground-based data were reduced using the standard or variant version of the image subtraction method (Alard & Lupton 1998; Wozniak 2000; Bramich 2008). The raw *K2* light curve was extracted and modeled following the method of Zhu et al. (2017a), which is a special application of Soares-Furtado et al. (2017) and Huang et al. (2015). The *Spitzer* data were reduced using the software that was customized for the microlensing program (Calchi Novati et al. 2015b).

## 3. Breaking Parallax Degeneracy with a Two-satellite Experiment

First, as a proof of concept of the two-satellite microlensing parallax method, we choose to only model the ground-based and *K2* data, and then compare the predicted *Spitzer* light curve with the actual *Spitzer* data.

The modeling of ground-based and *K2* data follows the methodology of Zhu et al. (2017a), but with a minor modification. According to the OGLE-III Catalog of Variable Stars (Soszyński et al. 2013), a low-amplitude (0.034 mag) long-period (342.5 days) variable, OGLE-BLG-LPV-202211, sits only 10$''$ (or 2.5 *K2* pixels) away from the location of MOA-2016-BLG-290. Due to the broad point-spread function and the unstable pointing of the *K2* spacecraft, this variable star affects the raw *K2* light curve that we extracted. Given the known phase of this variable from OGLE, we choose to introduce an additional term that scales linearly with time into the model of *K2* raw light curve (Equation (1) of Zhu et al. 2017a), in order to minimize the influence of the variable on the photometry. Following Zhu et al. (2017a), we also include a constraint on the source $K_p - I$ color, which is derived from the source $V - I$ color from OGLE photometry.

With only data from the ground and from *K2* included in the modeling, the fourfold degeneracy emerges. These are generally denoted as Earth–*K2* ($\pm$, $\pm$) solutions, with the first sign and the second sign indicating the sign of $u_{0,\oplus}$ and $u_{0,K2}$ in the geocentric frame, respectively (Zhu et al. 2015). The microlensing parameters for these solutions are given in Table 1, and the microlensing geometries are shown in

---

[28] Although the two-satellite microlensing experiment with *K2* and *Spitzer* is the first time that we observe the same event from three well-separated locations, it is not the first time that one event was observed by ground-based and two space-based telescopes. In 2015, a few *Spitzer* microlensing targets were also observed by *Swift*. See Shvartzvald et al. (2016) for the case of OGLE-2015-BLG-1319.

[29] The planetary event OGLE-2016-BLG-1190 presented in Ryu et al. (2017) was also observed by *K2*, *Spitzer*, and ground-based observatories, but the *K2* data did not detect the microlensing signal. Nevertheless, this nondetection also led to the resolution of the parallax degeneracy. See Ryu et al. (2017) for details.
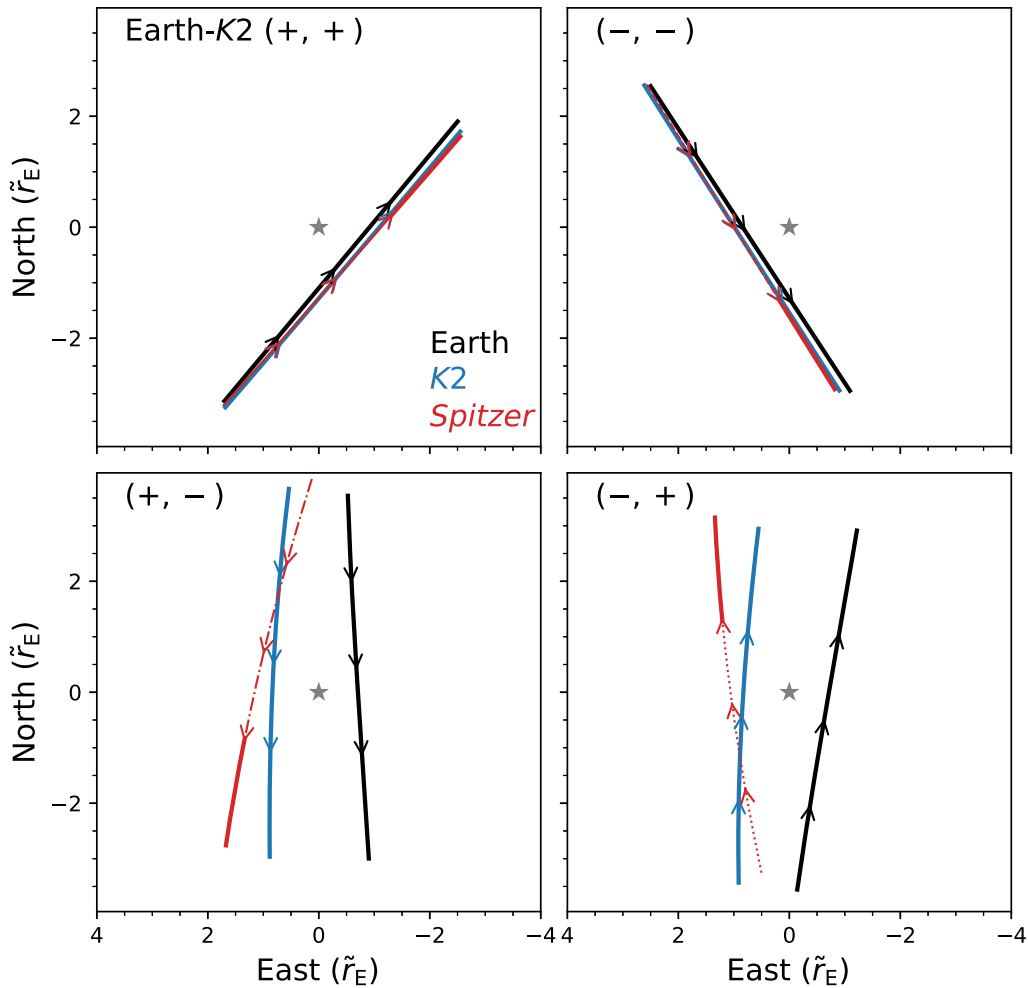
Figure 1. Trajectories of three observers (Earth, *K2*, and *Spitzer*) with respect to the aligned lens and source position (marked as stars). These are the *geocentric* views of microlensing geometries (Gould 2004). The four solutions allowed by the ground-based and *K2* data are shown individually, and the predicted *Spitzer* positions are shown in red, with the solid thick lines denoting the time span of actual *Spitzer* observations. For each trajectory, there are three arrows indicating the direction of motion at three different epochs: $HJD' = 7540$, 7550, and 7560, respectively. The trajectories are oriented so that north is up and east is left (see Skowron et al. 2011 for the sign convention of u_0). We note that the Earth–*K2*–*Spitzer* relative positions (in au) are the same in all plots, and that they are simply scaled differently in all plots for the given parallax measurements.

Table 1
Best-fit Parameters of Microlensing Models

Parameters	$(+, +)$	$(-, -)$	$(+, -)$	$(-, +)$
$t_{0,\oplus} - 7552$	0.380(4)	0.378(4)	0.375(4)	0.383(4)
$u_{0,\oplus}$	0.7032(6)	$-0.7033(6)$	0.7036(4)	$-0.7031(6)$
t_E (days)	6.370(8)	6.370(9)	6.379(9)	6.373(9)
$\pi_{E,N}$	0.180(5)	$-0.200(5)$	$-2.199(6)$	2.156(4)
$\pi_{E,E}$	$-0.150(4)$	$-0.131(4)$	$-0.139(4)$	$-0.370(4)$
$I - [3.6\,\mu m]$	$-5.29(13)$	$-5.35(13)$	$-4.89(13)$	$-4.53(13)$

Note. With only ground-based and *K2* data, all four solutions are allowed, but only the first two [$(+, +)$ and $(-, -)$] survive once *Spitzer* data and the the associated source $I - [3.6\,\mu m]$ color constraint are taken into account.

Figures 1 and 2 for different choices of the reference frame. As these plots illustrate, the four solutions are distinct in terms of the velocity vector of the lens-source relative motion, which is directly determined by the parallax vector π_E. If only the amplitude of parallax is considered, the fourfold degeneracy essentially collapses to twofold (Gould 1994), which we denote

as "small π_E" [$(+, +)$ and $(-, -)$] and "large π_E" [$(+, -)$ and $(-, +)$].

Because *Spitzer*'s position relative to Earth and *K2* is well known, we can then "predict" the microlensing light curve that *Spitzer* would see for all four solutions. These predicted *Spitzer* light curves are shown in the left panel of Figure 3 together with the ground-based (OGLE and MOA) and *K2* light curves. Given the different behaviors of the predicted light curves, *Spitzer* observations would in principle pick out the correct solution if this third observer had a full coverage of the event light curve. Unfortunately, *Spitzer* was not able to observe this event until $HJD' = 7559.5$ because of its Sun-angle limit, and therefore it only captured the falling tail of the light curve. Such a partial light curve can be fit by all four solutions equally well, if no other information is provided.

Fortunately, with the known properties of the source star, we are able to at least break the degeneracy in the parallax amplitude π_E (i.e., small π_E versus large π_E). The *Spitzer* (as well as OGLE and MOA) flux is modeled by

$$F(t) = F_S \cdot A(t) + F_B. \tag{2}$$
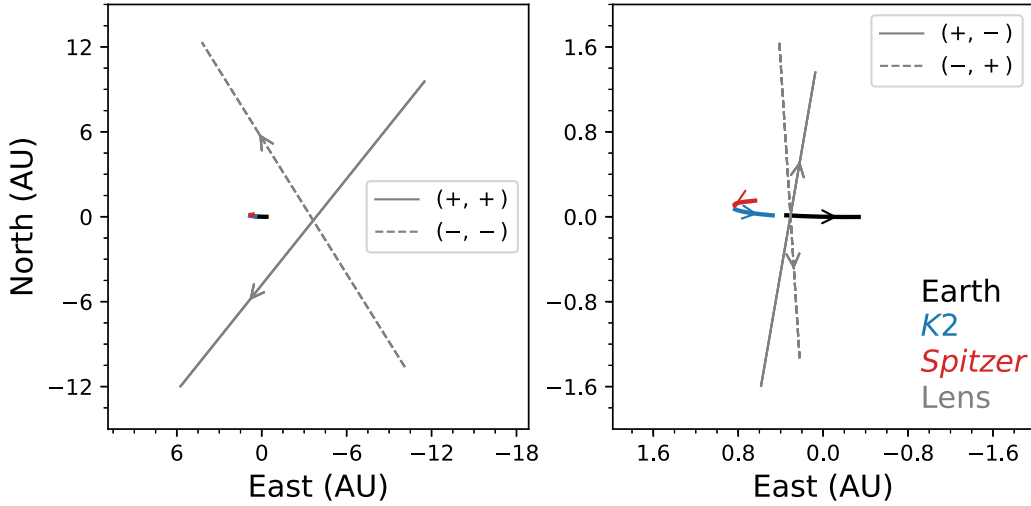
Figure 2. Trajectories of the lens with respect to the aligned source and observer (Earth at $t_{0,\oplus}$), and the motions of all three observers relative to the same reference point. These are the *heliocentric* views of microlensing geometries (Calchi Novati & Scarpetta 2016). Again, north is up and east is left, but we use the same physical scale for all solutions so that the motions of observers are the same. For each curve, the arrow indicates the position of the object as well as its directory of motion. Now the Earth-trailing orbits of *K2* and *Spitzer* are clearly seen.
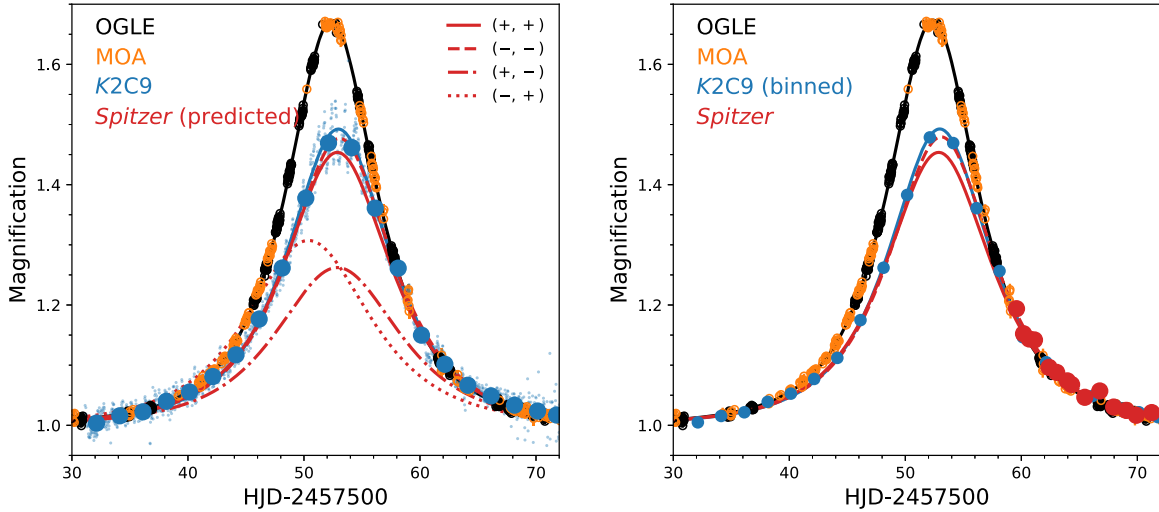
Figure 3. Left panel: predicted *Spitzer* light curves (in red) based on the modeling of the ground-based (OGLE in black and MOA in orange) and *K2*C9 (in blue) data. The raw *K2* data are shown as blue open dots, and the binned data are shown as blue solid dots with error bars. The four predicted *Spitzer* light curves are plotted with different line styles: solid, dashed, dashed–dotted, and dotted for Earth–*K2* $(+, +), (-, -), (+, -)$, and $(-, +)$ solutions, respectively. Right panel: data and the best-fit models for all observatories. Here, we only show the re-binned *K2*C9 data, and the remaining labels are the same as those in the left panel. Once all data and the color constraints are included, only the small π_E solutions, $(+, +)$ and $(-, -)$, are allowed.

Here, F_S is the source flux in the given observatory/bandpass, F_B is the flux that is within the aperture but that is irrelevant to the microlensing effect, and $A(t)$ is the microlensing magnification at given time t. For the same set of *Spitzer* measurements, a different magnification behavior would suggest a different source brightness F_S (and so source color $I - [3.6\,\mu\text{m}]$, since the source I magnitude is well determined). With the predicted *Spitzer* light curves from the previous step, the source $I - [3.6\,\mu\text{m}]$ colors are then estimated for all four solutions, and they are listed in Table 1 as well. The uncertainty on the source color is dominated by uncertainties on the *Spitzer* observations. For the two groups of solutions, the inferred source $I - [3.6\,\mu\text{m}]$ colors are statistically different at $>3\sigma$ level.

We then derive the source color

$$I - [3.6\,\mu\text{m}] = -5.56 \pm 0.12 \qquad (3)$$

from a model-independent way, by substituting the source $V - I$ color into the stellar $I - [3.6\,\mu\text{m}]$ versus the $V - I$ color–color relation. This relation is established based on neighboring field stars with similar properties (see details in Calchi Novati et al. 2015b). The deviations between this color measurement and inferred colors are $1.5\sigma, 1.2\sigma, 3.8\sigma$, and 5.8σ for $(+, +), (-, -), (+, -)$, and $(-, +)$ solutions, respectively. Therefore, the large π_E solutions can be securely rejected, and only the small π_E solutions are allowed. See Figure 4 for the illustration of the color determination and comparison.

As a final step, we model data from all observatories (OGLE, MOA, *K2*, and *Spitzer*) simultaneously. The microlensing parameters are almost identical to those for Earth–*K2* $(+, +)$ and $(-, -)$ solutions, and therefore are not listed separately here. The best-fit models and all data sets are illustrated in the right panel of Figure 3.
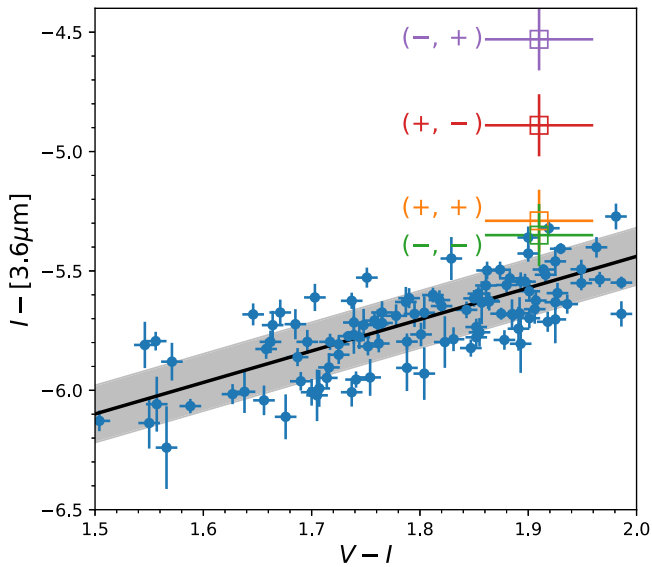
Figure 4. Stellar $I - [3.6 \,\mu\mathrm{m}]$ vs. $V - I$ color–color relation as well as the data points used to derive it. The shaded region remarks the 1σ uncertainty of this color–color relation. The open squares are the source colors inferred from the four solutions. The colors of the small π_E solutions ($++$ and $--$) are consistent with this independent color measurement, while those of the large π_E solutions ($+,-$ and $-,+$) are inconsistent at $>3\sigma$ level.

4. Discussion

In this work, we present the analysis of the first microlensing event that has detected signals from at least three well-separated ($\sim$1 au) locations, which in the current case are Earth, *K2*, and *Spitzer*. With data from the third well-separated observer, we have demonstrated that the generic parallax degeneracy arising in the single-satellite microlensing parallax experiment is effectively broken. This is essentially the first realization of the decades-old idea proposed by Refsdal (1966) and Gould (1994) independently.

For the current event, we could only break the degeneracy in the (twofold) parallax amplitude rather than the degeneracy in the (fourfold) parallax vector. This is partly because this event could not be observed by *Spitzer* until it was almost finished, but mostly because the event is near the ecliptic plane and the Earth–*K2*–*Spitzer* configuration is nearly colinear (Gaudi & Gould 1997). Nevertheless, it is the amplitude of the microlensing parallax that matters in determining the lens properties, and therefore being able to break the degeneracy in parallax amplitude has already enabled a better determination of the lens properties, such as the lens mass and distance. We use the current case as an example. For the large π_E solutions, the lens-source projected velocity $\tilde{v} = \mathrm{au}/(\pi_E t_E) = 1160 \,\mathrm{km\,s^{-1}}$, which indicates that the lens is mostly likely in the bulge (see the left panel of Figure 2 of Zhu et al. 2017b). For the small π_E solutions, however, this velocity is $130 \,\mathrm{km\,s^{-1}}$, and thus the lens should be in the near disk. More quantitatively, by using the Galactic model and the Bayesian method of Zhu et al. (2017b), we find that the lens of MOA-2016-BLG-290 has a mass $M_L = 77^{+34}_{-23} \, M_J$ and distance $D_L = 6.8 \pm 0.4 \,\mathrm{kpc}$ for accepted solutions (i.e., large π_E solutions). These values correspond to a brown dwarf or an extremely low-mass star likely in the Galactic bulge. However, the other two solutions, had they been correct, would suggest a high-mass ($7^{+4}_{-3} \, M_J$) planet in the near disk ($D_L = 2.5 \pm 0.8 \,\mathrm{kpc}$). The ability to

break the π_E amplitude degeneracy significantly reduces the uncertainties on the lens properties.

Among other proposed methods (Gould 1995, 1999; Gould & Yee 2012; Calchi Novati et al. 2015a; Yee et al. 2015b), obtaining observations from a third location has always been considered the most efficient in breaking the parallax degeneracy in satellite microlensing experiments. It is nevertheless difficult to do so for a large number of events for obvious economical reasons. In the absence of this method, the Rich argument can be applied for statistical purposes (Calchi Novati et al. 2015a; Zhu et al. 2017b). In fact, for the present case, the application of the Rich argument would also argue for an extremely low probability (1%) of the large π_E solutions. However, the resolution of degeneracy is important whenever precise knowledge is required of an individual event. Therefore, the $\sim$30 events observed in the 2016 two-satellite microlensing experiment are very valuable. This ensemble can be used to refine the microlensing parallax method, which is the foundation of the ongoing *Spitzer* microlensing project and will likely be a crucial component of the future space-based microlensing surveys.

Regardless, one may wonder when will be the next time to apply this two-satellite parallax method? Within the predictable period, one could only hope to apply this method one decade from now to the Wide Field InfaRed Survey Telescope (WFIRST; Spergel et al. 2015) and Euclid (Penny et al. 2013), although the situation will be largely different because these telescopes will likely be at the Earth–Sun L2 point (i.e., a much shorter baseline; see Zhu & Gould 2016 for a detailed analysis of WFIRST parallax; see also Yee 2013). Nevertheless, the history of the microlensing parallax has already proved that fantastic scientific ideas will never be buried.

ORCID iDs

Wei Zhu (祝伟) ⬤ https://orcid.org/0000-0003-4027-4711
C. X. Huang ⬤ https://orcid.org/0000-0003-0918-7484

References

Alard, C., & Lupton, R. H. 1998, ApJ, 503, 325
Bond, I. A., Abe, F., Dodd, R. J., et al. 2001, MNRAS, 327, 868
Bramich, D. M. 2008, MNRAS, 386, L77
Calchi Novati, S., Gould, A., Udalski, A., et al. 2015a, ApJ, 804, 20
Calchi Novati, S., Gould, A., Yee, J. C., et al. 2015b, ApJ, 814, 92
Calchi Novati, S., & Scarpetta, G. 2016, ApJ, 824, 109
Dong, S., Udalski, A., Gould, A., et al. 2007, ApJ, 664, 862
Gaudi, B. S., & Gould, A. 1997, ApJ, 477, 152
Gould, A. 1994, ApJL, 421, L75
Gould, A. 1995, ApJL, 441, L21
Gould, A. 1999, ApJ, 514, 869
Gould, A. 2004, ApJ, 606, 319
Gould, A., & Horne, K. 2013, ApJL, 779, L28
Gould, A., Yee, J., & Carey, S. 2015, sptz prop, 12015
Gould, A., & Yee, J. C. 2012, ApJL, 755, L17
Henderson, C. B., Poleski, R., Penny, M., et al. 2016, PASP, 128, 124401
Howell, S. B., Sobeck, C., Haas, M., et al. 2014, PASP, 126, 398
Huang, C. X., Penev, K., Hartman, J. D., et al. 2015, MNRAS, 454, 4159
Penny, M. T., Kerins, E., Rattenbury, N., et al. 2013, MNRAS, 434, 2
Refsdal, S. 1966, MNRAS, 134, 315
Ryu, Y.-H., Yee, J. C., Udalski, A., et al. 2017, ApJ, submitted
Shvartzvald, Y., Li, Z., Udalski, A., et al. 2016, ApJ, 831, 183
Shvartzvald, Y., Yee, J. C., Calchi Novati, S., et al. 2017, ApJL, 840, L3
Skowron, J., Udalski, A., Gould, A., et al. 2011, ApJ, 738, 87
Soares-Furtado, M., Hartman, J. D., Bakos, G. Á., et al. 2017, PASP, 129, 044501
Soszyński, I., Udalski, A., Szymański, M. K., et al. 2013, AcA, 63, 21
Spergel, D., Gehrels, N., Baltay, C., et al. 2015, arXiv:1503.03757
Street, R. A., Udalski, A., Calchi Novati, S., et al. 2016, ApJ, 819, 93
Udalski, A. 2003, AcA, 53, 291
Udalski, A., Szymanski, M., Kaluzny, J., et al. 1994, AcA, 44, 227
Udalski, A., Szymański, M. K., & Szymański, G. 2015, AcA, 65, 1
Udalski, A., Yee, J. C., Gould, A., et al. 2015, ApJ, 799, 237
Wozniak, P. R. 2000, AcA, 50, 421
Yee, J. C. 2013, ApJL, 770, L31
Yee, J. C., Gould, A., Beichman, C., et al. 2015a, ApJ, 810, 155
Yee, J. C., Udalski, A., Calchi Novati, S., et al. 2015b, ApJ, 802, 76
Zhu, W., & Gould, A. 2016, JKAS, 49, 93
Zhu, W., Huang, C. X., Udalski, A., et al. 2017a, PASP, 129, 104501
Zhu, W., Udalski, A., Calchi Novati, S., et al. 2017b, arXiv:1701.05191
Zhu, W., Udalski, A., Gould, A., et al. 2015, ApJ, 805, 8